NOTICE: This is the author's version of a work that was accepted for publication in Soil Dynamics and Earthquake Engineering. Changes resulting from the publishing process, such as peer review, editing, corrections, structural formatting, and other quality control mechanisms may not be reflected in this document. Changes may have been made to this work since it was submitted for publication. A definitive version was subsequently published in Soil Dynamics and Earthquake Engineering, Vol. 55, No. 12, pp. 130-139, 2013, DOI: 10.1016/j.soildyn.2013.08.006

Small-strain constrained elastic modulus of clean quartz sand with various grain size distribution

T. Wichtmann[i], Th. Triantafyllidis[ii]

Abstract: Approx. 120 resonant column (RC) tests with additional P-wave velocity measurements using piezoelectric elements have been performed on 19 clean quartz sands with piecewise linear, gap-graded, S-shaped or other smoothly shaped grain size distribution curves. For each material different pressures and densities were tested. It is demonstrated that the extended empirical equations for the small-strain constrained elastic modulus proposed by the authors in an earlier paper work well also for most of the more complex grain size distribution curves tested in the present study. These equations considering the influence of the uniformity coefficient of the grain size distribution curve were developed based on data from tests on linear gradations. A further improvement of the prediction for the more complex grain size distributions can be achieved if the correlation equations are applied with a specially defined average inclination of the grain size distribution curve. Such improvement is demonstrated not only for the small-strain constrained elastic modulus, but also for small-strain shear modulus, modulus degradation and Poisson's ratio.

Keywords: P-wave velocity; small strain constrained elastic modulus; quartz sand; grain size distribution curve; uniformity coefficient

1 Introduction

Similar to the small strain shear modulus $G_{\max}$ (Iwasaki & Tatsuoka [8], Wichtmann & Triantafyllidis [9]), the small-strain constrained elastic modulus $M_{\max}$ of clean quartz sand is strongly dependent on the uniformity coefficient $C_u = d_{60}/d_{10}$ of the grain size distribution curve (Wichtmann & Triantafyllidis [10]). For constant values of void ratio and pressure, $G_{\max}$ and $M_{\max}$ decrease with increasing C_u, while they are rather independent of mean grain size d_{50}. The common empirical formulas for the small-strain stiffness were developed based on tests on rather uniform sands. It has been demonstrated that these equations should not be applied to well-graded granular materials since they may strongly overestimate the stiffness of well-graded soils [9, 10].

In order to consider the influence of the uniformity coefficient in an empirical formula for $M_{\max}$, the authors [10] have proposed the following set of equations, based on the well-known empirical formula of Hardin [5, 7]:

$$M_{\max} = A \, \frac{(a-e)^2}{1+e} \left(\frac{p}{p_{\text{atm}}}\right)^n p_{\text{atm}} \qquad (1)$$

$$a = 2.16 \, \exp(-0.055 \, C_u) \qquad (2)$$

$$n = 0.344 \, {C_u}^{0.126} \qquad (3)$$

$$A = 3655 + 26.7 \, {C_u}^{2.42} \qquad (4)$$

with void ratio e, mean effective confining pressure p and atmospheric pressure $p_{\text{atm}} = 100$ kPa. The correlations (2) to (4) are based on 163 resonant column (RC) tests with P-wave measurements performed on 25 grain size distribution curves with linear shape in a diagram with semi-logarithmic scale. The testing methodology was the same as that applied in the present study (see next section). As an alternative to Eqs. (1) to (4), a relationship between $M_{\max}$ and relative density D_r has been established in [10]:

$$M_{\max} = 2316 \, (1 + 1.07 \, D_r[\%]/100) \, {p_{\text{atm}}}^{1-0.39} \, p^{0.39} \qquad (5)$$

with $D_r = (e_{\max} - e)/(e_{\max} - e_{\min})$ calculated with the minimum and maximum void ratios $e_{\min}$ and $e_{\max}$ from standard tests (determined according to DIN 18126 in case of the present study).

The present paper investigates whether the extended empirical equations (1) to (5) can be also applied to more complex grain size distribution curves. For this purpose experimental data collected for piecewise linear, gap-graded, S-shaped and other smoothly shaped grain size distribution curves are analyzed.

2 Tested material, test device and testing procedure

The specially omposed grain size distribution curves tested in the present study are collected in Figure 1. They are also shown separately in the first and third column of diagrams in Figures 5 and 6. The original material is a natural quartz sand with subangular grains originating from a sand pit near Dorsten, Germany. Some of the grain size distribution curves (materials PL1 - PL7) have a piecewise linear shape with varying inclinations and inflection points. Others are gap-graded (materials GG1 - GG8) with varying span of missing grain sizes. S-shaped and other smoothly shaped grain size distribution curves (materials S2 - S6) were also tested. The values of mean grain size d_{50}, uniformity coefficient C_u and curvature index $C_c = (d_{30})^2/(d_{10}d_{60})$ of the tested grain size distribution curves are given in Table

[i] Researcher, Institute of Soil Mechanics and Rock Mechanics, Karlsruhe Institute of Technology, Germany (corresponding author). Email: torsten.wichtmann@kit.edu

[ii] Professor and Director of the Institute of Soil Mechanics and Rock Mechanics, Karlsruhe Institute of Technology, Germany

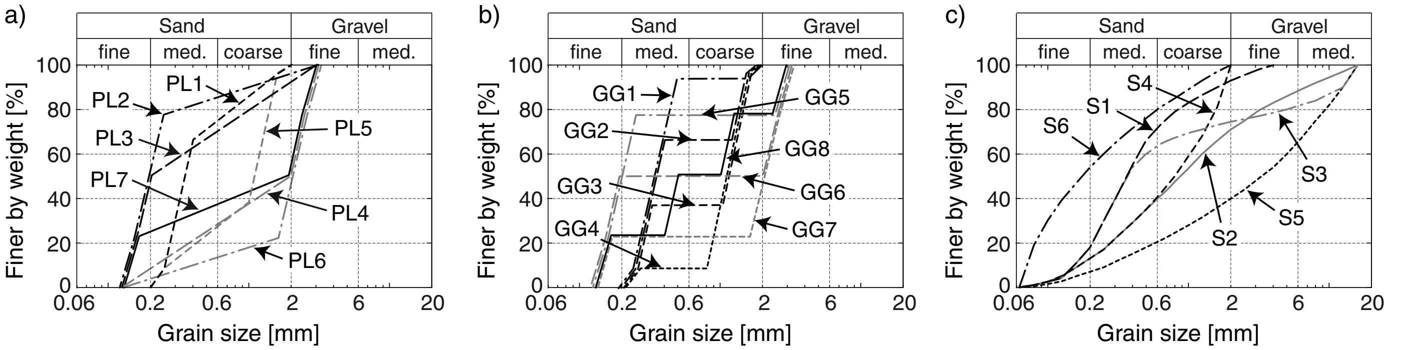

Fig. 1: *Specially composed grain size distribution curves tested in the present study*

Material	d_{50} [mm]	C_u [-]	$C_{u,A}$ [-]	C_c [-]
PL1	0.35	1.5	1.95	0.92
PL2	0.2	1.5	2.16	0.96
PL3	0.2	2.5	3.2	0.6
PL4	2.0	10.0	7.7	0.92
PL5	1.1	4.5	4.2	1.45
PL6	2.0	5.6	5.6	3.43
PL7	2.0	15.6	9.8	3.3
GG1	0.35	1.5	1.64	0.92
GG2	0.35	1.5	2.42	0.92
GG3	1.1	4.7	3.7	0.29
GG4	1.1	1.5	1.29	0.92
GG5	0.2	1.5	3.0	0.96
GG6	2.0	15.6	6.6	0.1
GG7	2.0	15.5	14.6	6.12
GG8	1.0	7.8	7.1	1.19
S1	0.37	2.9	3.5	0.91
S2	0.89	7.4	8.7	0.82
S3	0.37	3.2	6.8	0.81
S4	0.8	6.1	5.4	0.99
S5	3.3	18.5	15.2	0.96
S6	0.18	3.5	4.1	0.56

Table 1: Mean grain size d_{50}, uniformity coefficient C_u, average inclination $C_{u,A}$ and curvature index C_c of the tested grain size distribution curves

1. $M_{\max}$ data was not available for the materials GG7 and S5, for which $G_{\max}$ data has been analyzed by the authors in [12].

A scheme of the resonant column (RC) device used for the present study is shown in Fig. 2. It is of the "free - free" type, meaning both the top and the base mass are freely rotatable. The cuboidal top mass is equipped with two electrodynamic exciters each accelerating a small mass. This acceleration and the resulting acceleration of the top mass are measured with acceleration transducers. From these signals the torsional moment $M(t)$ and the angle of twist $\theta(t)$ at the top of the sample can be calculated. The sample is enclosed in a pressure cell. The state of stress is almost isotropic. A small stress anisotropy results from the weight of the top mass ($m \approx 9$ kg), such that the vertical stress σ_1 is slightly higher than the lateral one σ_3. However, for higher cell pressures this anisotropy is of secondary importance. Furthermore, test results of Yu & Richart [14] reveal that a stress anisotropy becomes significant only near failure.

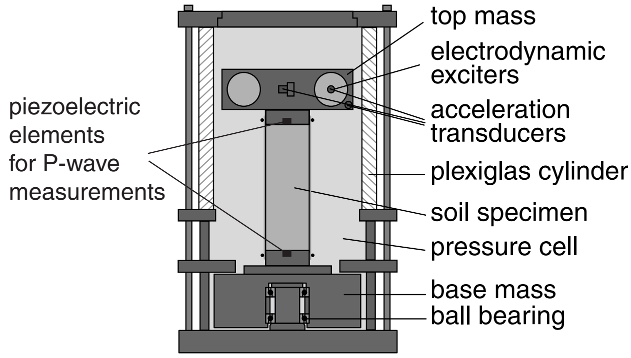

Fig. 2: *Scheme of the Resonant Column device used for the present study*

A sinusoidal electrical signal is generated by a function generator, amplified and applied to the electrodynamic exciters. The frequency of excitation is varied until the resonant frequency f_R of the system composed of the two end masses and the specimen has been found. By definition, this is the case when $M(t)$ and $\theta(t)$ have a phase-shift of $\pi/2$ in time t. The secant shear modulus

$$G \quad = \quad \left(\frac{2\pi\ h\ f_R}{a}\right)^2 \varrho \tag{6}$$

is calculated from the resonant frequency, the height h and the density ϱ of the specimen. The parameter a is obtained from Eq. (7):

$$a\ \tan(a) \ - \ \frac{J^2}{J_0\ J_L}\ \frac{\tan(a)}{a} \quad = \quad \frac{J}{J_0} \ + \ \frac{J}{J_L} \tag{7}$$

In Eq. (7) J is the polar mass moment of inertia of the specimen and $J_0 = 1.176$ kg m^2 and $J_L = 0.0663$ kg m^2 are the respective values of the base mass and the top mass (Fig. 2a).

Different shear strain amplitudes can be tested by varying the amplitude of the torsional excitation. All tested specimens had a full cross section and measured $d = 10$ cm in diameter and $h = 20$ cm in height. The variation of the shear strain amplitude with radius r is considered by calculating a mean value over the sample volume:

$$\bar{\gamma} \quad = \quad \frac{1}{V} \int\limits_V \gamma(r,x)\ \mathrm{d}V \tag{8}$$

This mean value is simply denoted by γ in the analysis of the test results in this paper. The shear strain amplitudes

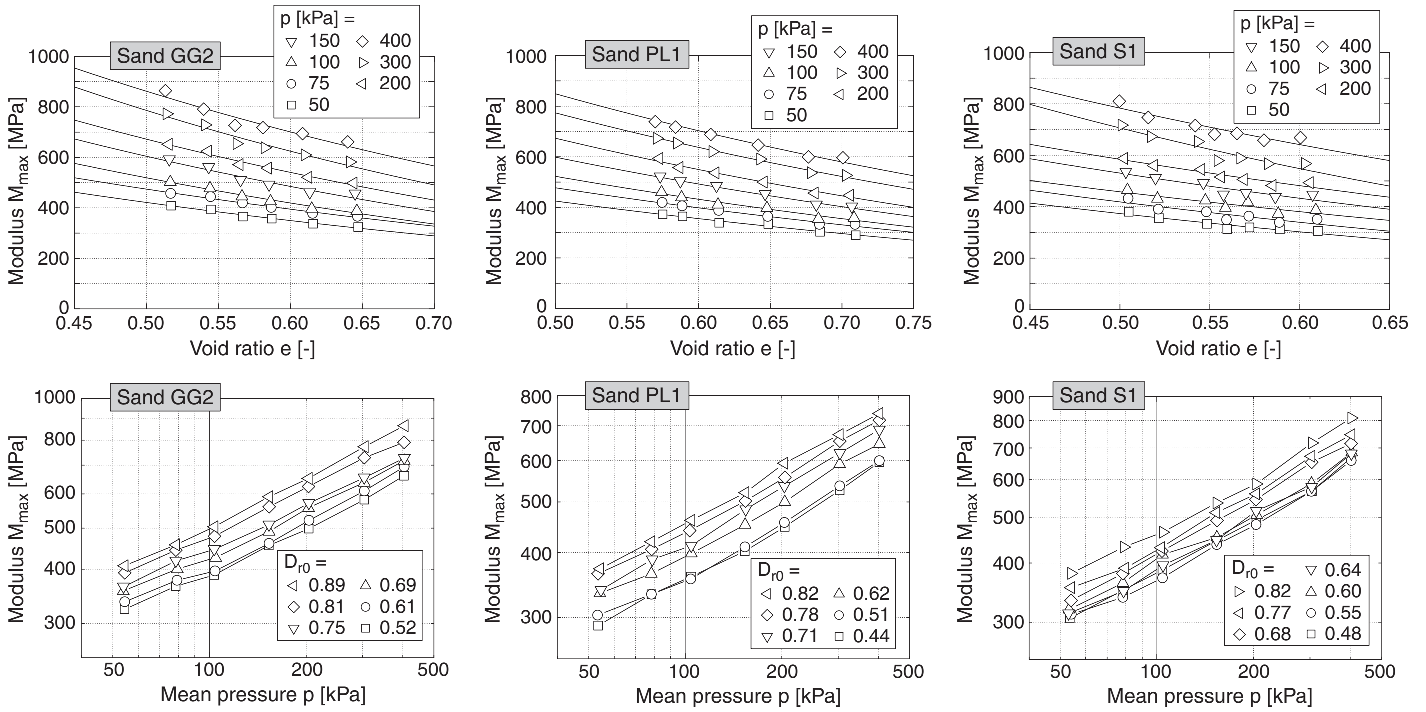

Fig. 4: *Small-strain constrained elastic modulus $M_{\max}$ as a function of void ratio for different confining pressures (upper row of diagrams) and as a function of confining pressure for different initial relative densities (lower row of diagrams). The data is shown for a piecewise linear (PL1), a gap-graded (GG2) and an S-shaped (S1) grain size distribution curve.*

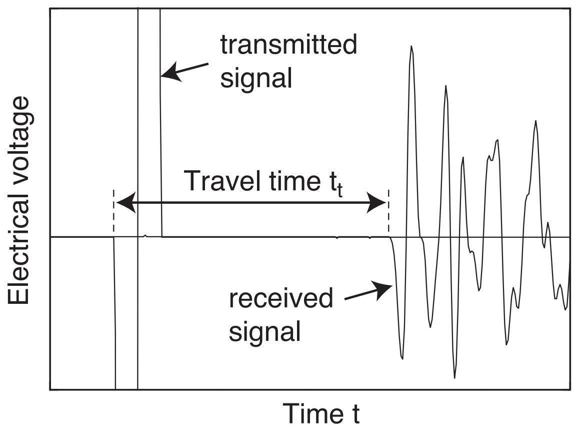

Fig. 3: *Example of transmitted and received signals, interpretation of travel time t_t, from [10]*

that can be tested in the RC device lie in the range $5 \times 10^{-7} \leq \gamma \leq 5 \times 10^{-4}$.

For P-wave measurements the specimen end plates have been additionally equipped with piezoelectric elements. The transducers are similar to those explained by Brignoli et al. [4]. A single sinusoidal signal with a frequency of f = 20 kHz was applied to the element in the base pedestal. The travel time t_t has been determined from the first arrival of the signal received at the top cap. Typical signals are presented in Figure 3.

Delay times in cables, amplifiers, etc. have been subtracted from t_t. Based on the literature the strain amplitudes generated in the soil using this type of P-wave sensors are assumed to be less than 10^{-6}. The constrained elastic modulus is calculated from the P-wave velocity using $M_{\max} = \varrho(v_P)^2$ with soil density ϱ. In [13] it has been demonstrated that the $G_{\max}$-values obtained from S-wave velocity measurements by means of piezoelectric elements are close to the $G_{\max}$-values measured with the RC device. Therefore, the $G_{\max}$ values obtained with the RC function of the test device and the $M_{\max}$ values derived from the P-wave measurements can be directly compared in order to calculate Poisson's ratio.

The lateral deformations and the settlement of the samples due to the increase of confining pressure or the application of shear strain cycles with higher amplitude γ were measured with non-contact displacement transducers.

All specimens were prepared by air pluviation and tested in the air-dry condition. For each material several specimens with different initial relative densities D_{r0} were tested. The mean effective confining pressure p was increased step-wise from $p = 50$ to 400 kPa. At each pressure p the small strain shear modulus $G_{\max}$ and the P-wave velocity v_P were measured after a resting period of 5 minutes, in order to obtain a similar "aging" (Afifi & Woods [2], Afifi & Richart [1], Baxter [3]) of the samples. Finally, the curves $G(\gamma)$ and $D(\gamma)$ were measured at $p = 400$ kPa. In three additional tests on medium dense specimens the modulus degradation and the damping ratio were also measured at $p = 50$, 100 and 200 kPa for each material.

3 Test results for small-strain constrained elastic modulus

Typical test results for a piecewise linear (PL1), a gap-graded (GG2) and an S-shaped (S1) grain size distribution curve are shown in Figure 4. The upper row of diagrams in Figure 4 gives the small-strain constrained elastic modulus $M_{\max}$ as a function of void ratio for different confining pres-

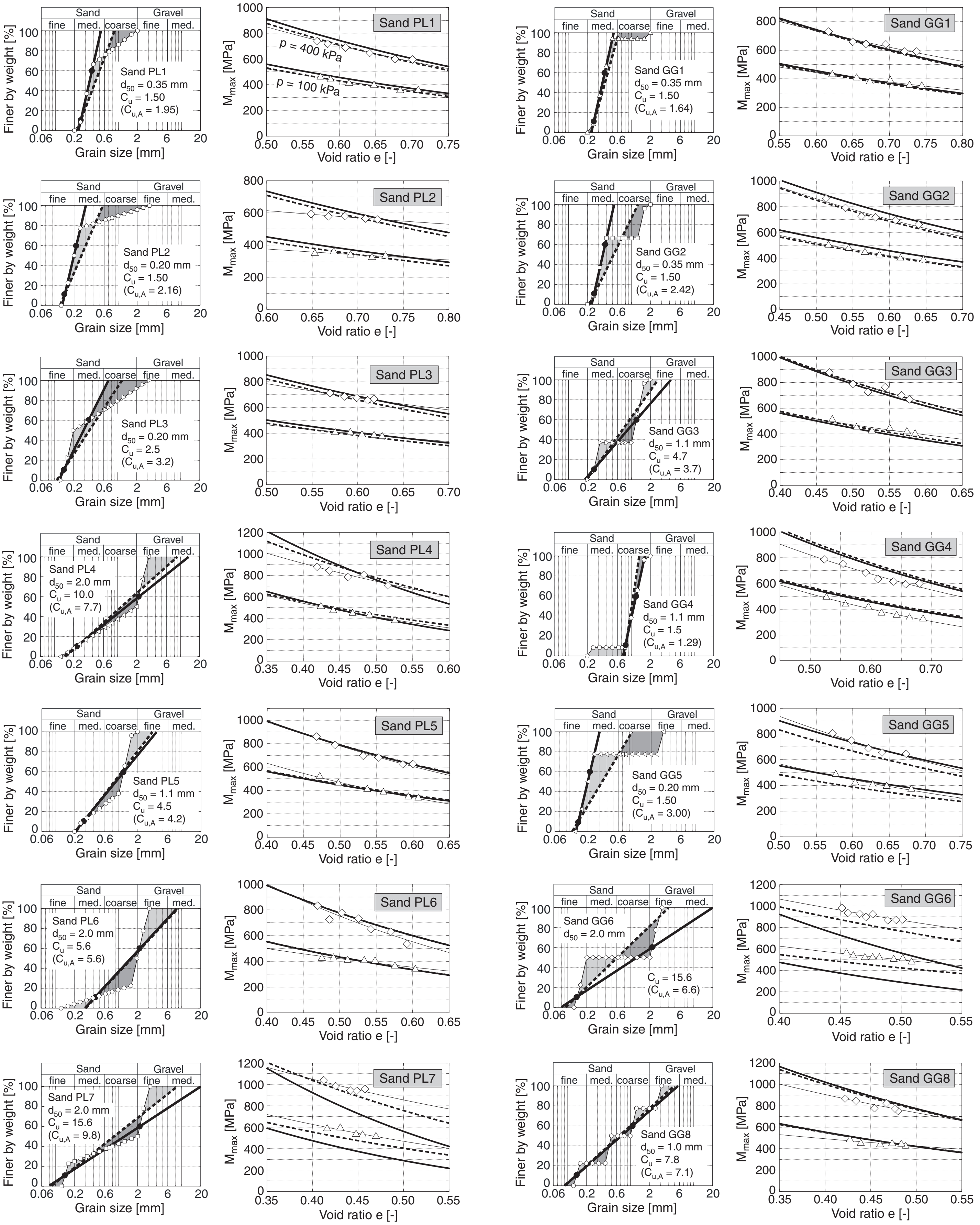

Fig. 5: *Small-strain constrained elastic modulus $M_{\max}(e)$ for piecewise linear and gap-graded grain size distribution curves: Comparison of test data for pressures $p = 100$ and 400 kPa with data predicted by Eqs. (1) to (4) using either C_u (thick solid curves) or $C_{u,A}$ (dashed curves) as input for the correlations. The thin solid curves are the best-fit curves of Eq. (1) for the data at pressure $p = 100$ or 400 kPa, respectively.*

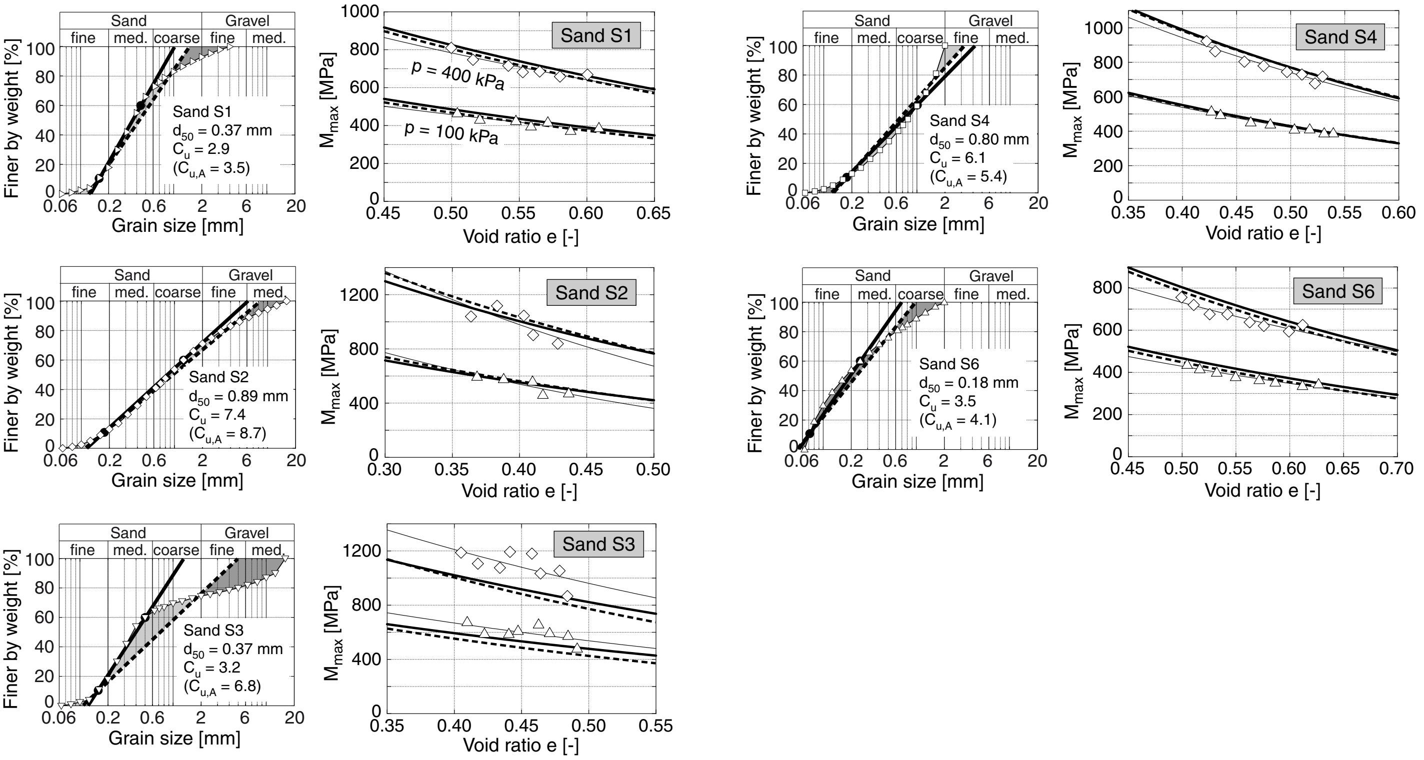

Fig. 6: *Small-strain constrained elastic modulus $M_{\max}(e)$ for smoothly shaped grain size distribution curves: Comparison of test data for pressures $p = 100$ and 400 kPa with data predicted by Eqs. (1) to (4) using either C_u (thick solid curves) or $C_{u,A}$ (dashed curves) as input for the correlations. The thin solid curves are the best-fit curves of Eq. (1) for the data at pressure $p = 100$ or 400 kPa, respectively.*

sures, while the diagrams in the lower row contain $M_{\max}$ data for various initial relative densities versus confining pressure. Figure 4 confirms the expected decrease of $M_{\max}$ with increasing void ratio and the power-law relationship $M_{\max} \sim p^n$ between small-strain constrained elastic modulus and effective confining pressure p. The increase of $M_{\max}$ with decreasing void ratio and increasing pressure is also obvious in the second and fourth column of diagrams in Figures 5 and 6, where $M_{\max}(e)$ data for pressures $p = 100$ and 400 kPa is provided for all tested materials.

In Figure 7 the small-strain constrained elastic modulus $M_{\max}$ at a void ratio $e = 0.55$ is plotted versus the uniformity coefficient C_u for mean pressures $p = 100$ and 400 kPa. These $M_{\max}$-values have been interpolated or carefully extrapolated based on the data shown in Figures 5 and 6. Only materials with $M_{\max}$ data near $e = 0.55$ have been considered in Figure 7. The data from the current tests (filled circles in Figure 7) are compared with results obtained by the authors [10] for linear grain size distribution curves (open symbols in Figure 7). Similar as in the tests on the linear grain size distribution curves, a significant decrease of $M_{\max}$ with increasing C_u was also observed in the present test series.

The small-strain constrained elastic moduli $M_{\max}(e)$ predicted by Eqs. (1) to (4) for $p = 100$ and 400 kPa have been added as thick solid curves in the second and fourth column of diagrams in Figures 5 and 6. These curves were generated using C_u as input for the correlations (2) to (4). The equivalent linear grain size distribution curves, which have the same d_{10}- and C_u-values as the tested grain size distribution curves, are shown as thick solid lines in the

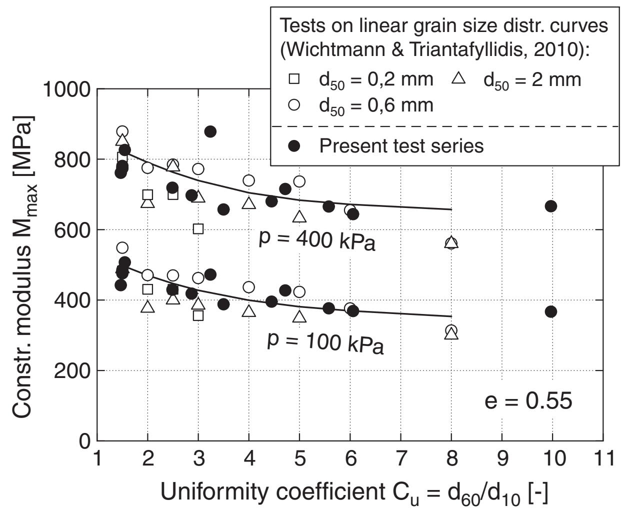

Fig. 7: *Small strain constrained elastic modulus $M_{\max}$ for a void ratio $e = 0.55$ and pressures $p = 100$ and 400 kPa as a function of uniformity coefficient C_u; Comparison of data from the present test series (filled circles) with data measured for linear grain size distribution curves (open symbols, [10])*

first and third column of diagrams in Figures 5 and 6. For most of the more complex grain size distribution curves, the experimental data is well approximated by Eqs. (1) to (4). The measured moduli of some materials (e.g. PL1, PL2, PL4, GG2, GG4, GG8, S4 and S6) are slightly overestimated by Eqs. (1) to (4) while the moduli of other materials (e.g. S3) are slightly underestimated. A relatively large un-

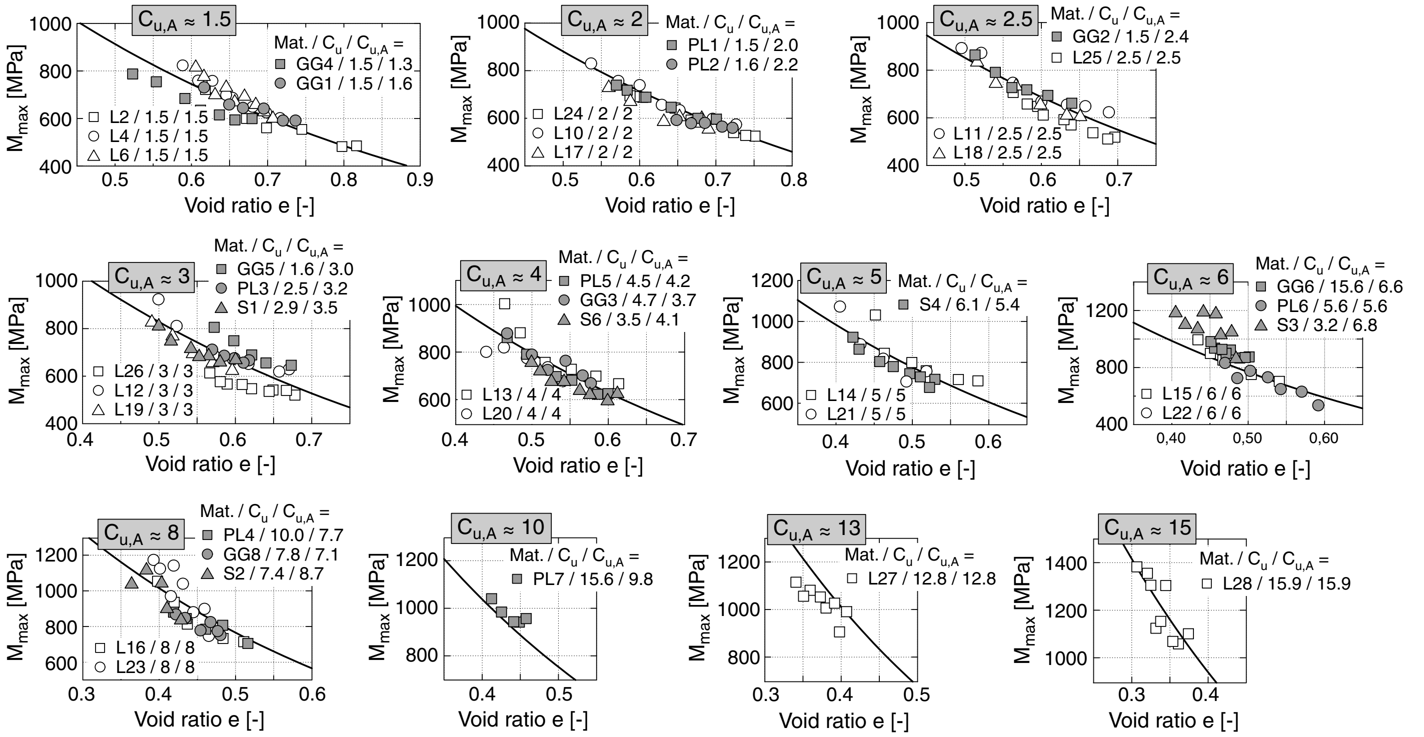

Fig. 8: *Small strain constrained elastic modulus $M_{\max}$ as a function of void ratio e for p = 400 kPa. Each diagram collects the $M_{\max}(e)$ data for certain $C_{u,A}$ values. The data for the linear grain size distribution curves L2 to L28 (taken from [10]) are in good accordance with the data for the more complex grain size distribution curves tested in the present study. The solid curves in the diagrams have been generated with Eqs. (1) to (4).*

derestimation of the experimental $M_{\max}$ data (up to factor 1.7) was observed for the two materials PL7 and GG6.

An improvement of the $M_{\max}$ prediction, in particular for the materials PL7 and GG6, can be achieved if the correlations (2) to (4) are applied with an average inclination $C_{u,A}$ of the grain size distribution curve. The definition of $C_{u,A}$ is explained in Figure 9, using the grain size distribution curve of sand PL2 as an example. While the equivalent linear gradation has the same d_{10} value as the tested grain size distribution curve, its inclination $C_{u,A}$ is chosen such way that the areas enclosed between the tested and the equivalent linear curve, above and below the tested curve, are equal in the semi-logarithmic scale ($A_1 = A_2$ in Figure 9). The equivalent linear gradations with inclination $C_{u,A}$ are shown as dashed thick lines in the first and third column of diagrams in Figures 5 and 6. The $C_{u,A}$-values are collected in Table 1 and are also specified in Figures 5 and 6. For most tested materials, in particular for PL7 and GG6, the differences between the measured and the predicted $M_{\max}$-values are less if $C_{u,A}$ is used instead of C_u. This becomes also clear from Table 2 where the percentage of predicted $M_{\max}$ data differing either ≤ 10% or ≤ 20% from the measured $M_{\max}$ data is provided. For comparison, in Table 2 similar data is given for the linear grain size distribution curves tested by the authors [10].

Another proof for the good prediction quality of the extended empirical equations is provided in Figure 8. Each diagram in Figure 8 collects the $M_{\max}(e)$ data at $p = 400$ kPa for certain $C_{u,A}$ values, measured for the linear or the more complex grain size distribution curves (for the linear curves $C_u = C_{u,A}$ holds). The experimental data for both types of gradations is well approximated by the curves $M_{\max}(e)$

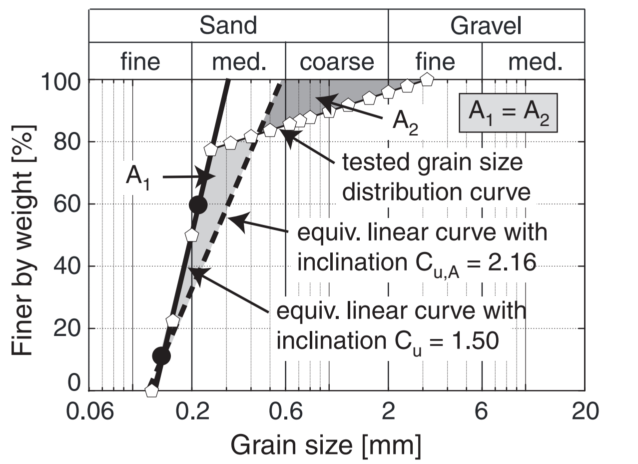

Fig. 9: *Grain size distribution curve of sand PL2 and equivalent linear grain size distribution curves with inclinations C_u or $C_{u,A}$, respectively*

	Eqs. (1)-(4) with C_u		Eqs. (1)-(4) with $C_{u,A}$		Eq. (5)	
	≤ 10%	≤ 20%	≤ 10%	≤ 20%	≤ 10%	≤ 20%
This study	72	89	76	96	60	80
Linear [10]	75	97	75	97	43	70

Table 2: Percentage values of predicted $M_{\max}$ data differing either ≤ 10% or ≤ 20 % from the experimental data. These values are mean values over all tested materials with either linear (second row) or more complex (first row) grain size distribution.

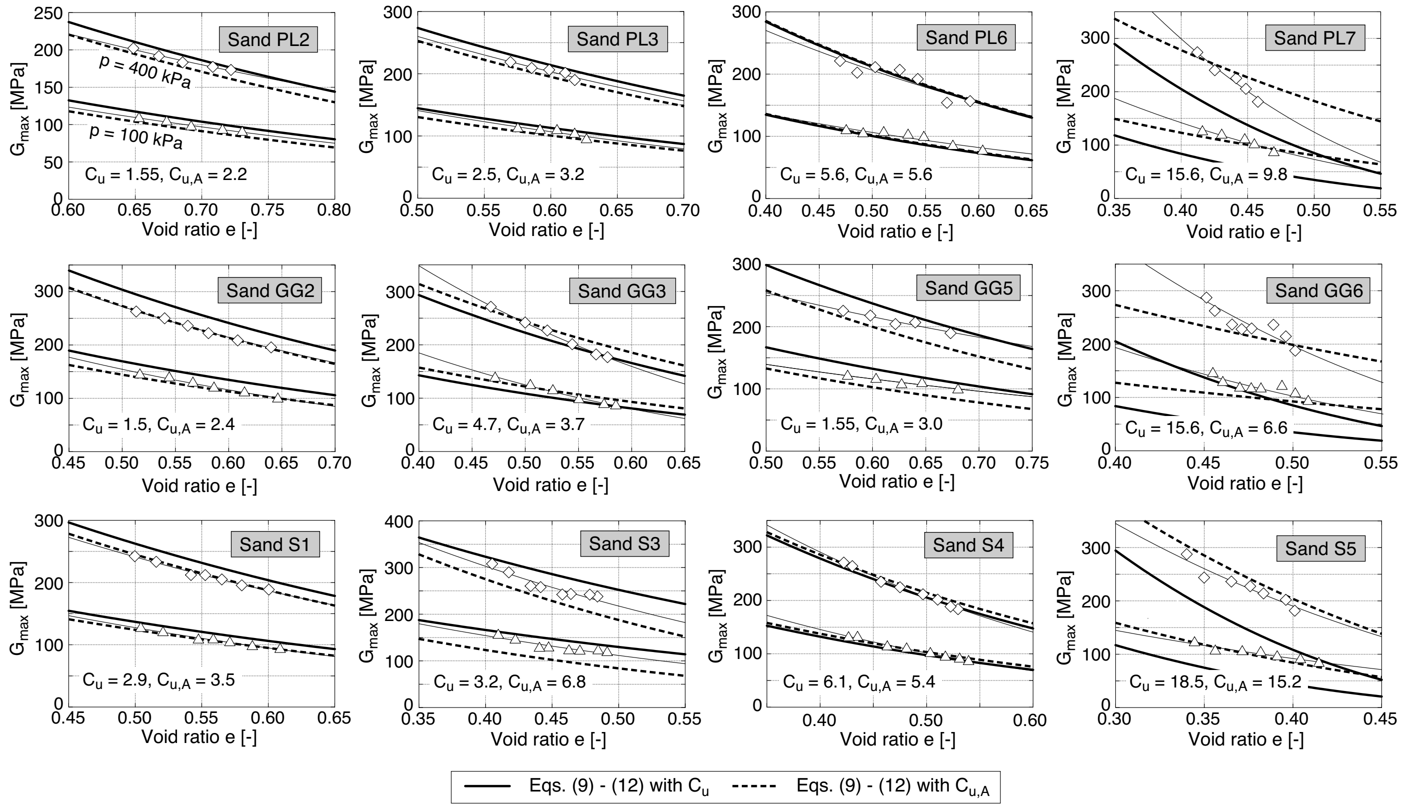

Fig. 10: *Small strain shear modulus $G_{\max}(e)$ for stepwise linear (first row), gap-graded (second row) and smoothly shaped (third row) grain size distribution curves. The experimental data is compared to $G_{\max}$ data predicted by Eqs. (9) to (12). The correlations have been applied either with C_u (thick solid curves) or $C_{u,A}$ (thick dashed curves). (Figure 2 from [12] supplemented by the dashed curves)*

predicted by Eqs. (1) to (4) applied with $C_{u,A}$ (solid curves in Figure 8).

In agreement with the results for linear grain size distribution curves [10], the values in the last two columns of Table 2 demonstrate that the prediction by Eq. (5) using relative density D_r as input is much less accurate than that of Eqs. (1) to (4) with either C_u or $C_{u,A}$.

4 Reanalysis of small-strain shear modulus and modulus degradation data in terms of average inclination of grain size distribution curve

In [12] the authors presented the data of small-strain shear modulus $G_{\max}$ and modulus degradation ratio $G(\gamma)/G_{\max}$ measured for the grain size distribution curves shown in Figure 1. Since an improved $M_{\max}$ prediction was found for the more complex grain size distribution curves if the correlations (2) to (4) were applied with the average inclination $C_{u,A}$ instead of the conventional C_u, a possible improvement by using $C_{u,A}$ was also inspected for $G_{\max}$ and $G(\gamma)/G_{\max}$, re-analyzing the data from [12].

Figure 10 presents the experimental $G_{\max}(e)$ data at pressures $p = 100$ and 400 kPa for some of the tested sands. The prediction by the equation (Hardin [5, 7])

$$G_{\max} = A \frac{(a-e)^2}{1+e} \left(\frac{p}{p_{\text{atm}}}\right)^n p_{\text{atm}} \tag{9}$$

with the correlations (10) to (12) proposed by the authors in [9]

$$a = 1.94 \exp(-0.066\ C_u) \tag{10}$$

$$n = 0.40\ {C_u}^{0.18} \tag{11}$$

$$A = 1563 + 3.13\ {C_u}^{2.98} \tag{12}$$

has been added as thick solid curves in Figure 10. Eqs. (10) to (12) have been evaluated with C_u for generating these curves. The prediction by Eqs. (9) to (12) using $C_{u,A}$ instead of C_u is provided as thick dashed curves in Figure 10. For most of the tested materials, the prediction with $C_{u,A}$ lies closer to the experimental data than the curves generated with C_u. In particular, an improvement of the $G_{\max}$ prediction can be achieved for sands PL7, GG8 and S5, which either contain a large amount of gravel (about 60 % in the case of S5) or are primarily composed of two components with significantly different grain size (fine sand and fine gravel in case of PL7 and GG6).

A quantitative analysis of the differences between measured and predicted $G_{\max}$ data is provided in Table 3, where the percentage values of predicted $G_{\max}$ data differing either $\leq$ 10% or $\leq$ 20% from the measured data are given. The differences between measured and predicted data are less if $C_{u,A}$ is applied in the prediction instead of C_u. For comparison, the values for the linear grain size distribution curves tested by the authors [9] are also provided in Table 3.

Another proof for the good prediction quality of Eqs. (9) to (12) with the average inclination $C_{u,A}$ is provided in Figure 11 where the $G_{\max}(e)$ data for $p = 400$ kPa is presented in a similar manner as the $M_{\max}(e)$ data in Figure 8. Each diagram in Figure 11 collects the shear moduli measured for sands having a similar $C_{u,A}$-value. For $C_{u,A} \approx$ constant,

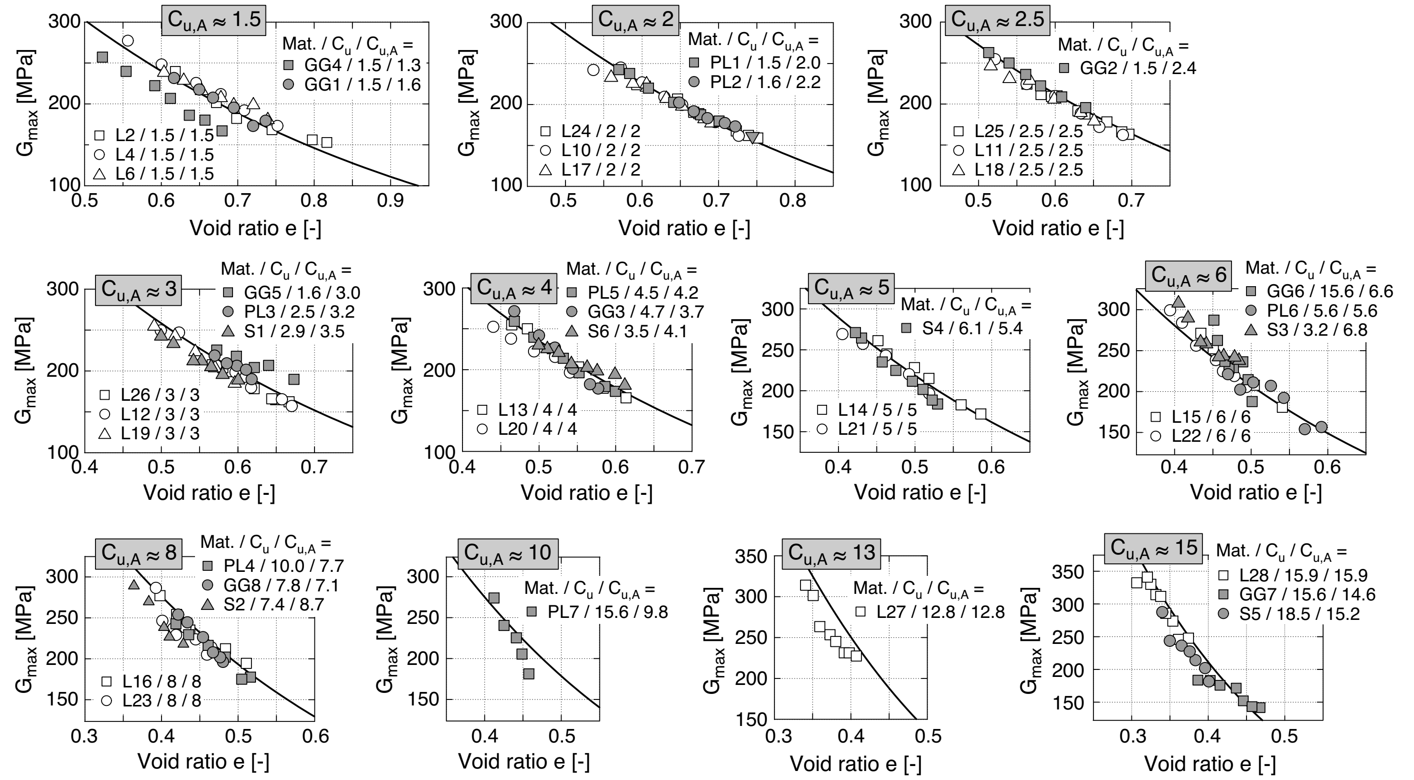

Fig. 11: *Small strain shear modulus $G_{\max}$ as a function of void ratio e for p = 400 kPa. Each diagram collects the $G_{\max}(e)$ data for certain $C_{u,A}$ values. The data for the linear grain size distribution curves L2 to L28 (taken from [9]) are in good accordance with the data for the more complex grain size distribution curves. The solid curves in the diagrams have been generated with Eqs. (9) to (12).*

	Eqs. (9)-(12) with C_u		Eqs. (9)-(12) with $C_{u,A}$	
	$\leq 10\%$	$\leq 20\%$	$\leq 10\%$	$\leq 20\%$
This study	55	80	73	94
Linear [9]	88	99	88	99

Table 3: Percentage values of predicted $G_{\max}$ data differing either $\leq 10\%$ or ≤ 20 % from the experimental data. These values are mean values over all tested materials with either linear (second row) or more complex (first row) grain size distribution.

	Eqs. (13)+(14) with C_u		Eqs. (13)+(14) with $C_{u,A}$	
	≤ 0.05	≤ 0.1	≤ 0.05	≤ 0.1
This study	77	96	81	98
Linear [11]	86	99	86	99

Table 4: Percentage values of predicted $G/G_{\max}$ data differing ≤ 0.05 or ≤ 0.1 from measured $G/G_{\max}$ data. Only data with $G/G_{\max} < 0.9$ is considered. These values are mean values over all tested materials with either linear (second row) or more complex (first row) grain size distribution.

the $G_{\max}(e)$ data of the various tested sands is similar - irrespectively if the grain size distribution curve is linear or more complex. The experimental data is well approximated by Eqs. (9) to (12) if the correlations are applied with $C_{u,A}$ (see the solid curves in Figure 11).

The modulus degradation curves $G(\gamma)/G_{\max}$ measured for some of the tested materials at pressures p = 50 and 400 kPa are shown in Figure 12. The prediction by the empirical formula proposed by Hardin & Drnevich [6]

$$\frac{G}{G_{\max}} = \frac{1}{1+\frac{\gamma}{\gamma_r}\left[1+a\ \exp\left(-\frac{\gamma}{\gamma_r}\right)\right]} \tag{13}$$

with the correlation developed by the authors in [11]

$$a = 1.070\ \ln(C_u) \tag{14}$$

has been added as thick solid curves in Figure 12, using C_u as input for the correlation. The reference shear strain $\gamma_r = \tau_{\max}/G_{\max}$ has been evaluated using $\tau_{\max} = p\ \sin\varphi_P$ for isotropic stress conditions, applying the following correlation for the peak friction angle φ_P proposed in [11]:

$$\varphi_P = 34.0^\circ\ \exp(0.27\ (D_r[\%]/100)^{1.8}) \tag{15}$$

If Eq. (14) is evaluated with $C_{u,A}$ instead of C_u, the thick dashed curves shown in Figure 12 are obtained. For most of the tested materials, the differences between the $G(\gamma)/G_{\max}$ predictions using either C_u or $C_{u,A}$ are small. However, for the materials PL7, GG6 and S5 a better approximation of the experimental data can be achieved if the correlation (14) is applied with $C_{u,A}$ as input. The slightly better approximation of the experimental data with $C_{u,A}$ instead of C_u becomes clear also from Table 4 where the percentage values of predicted $G(\gamma)/G_{\max}$ data differing either ≤ 0.05 or ≤ 0.1 from the measured data is provided. The respective values for linear gradations [11] are given for comparison in Table 4.

Based on the data in Figures 10 and 12 it can be concluded that similar as in the case of $M_{\max}$ also the $G_{\max}$ and $G(\gamma)/G_{\max}$ predictions for more complex grain size distribution curves can be improved if the correlations derived

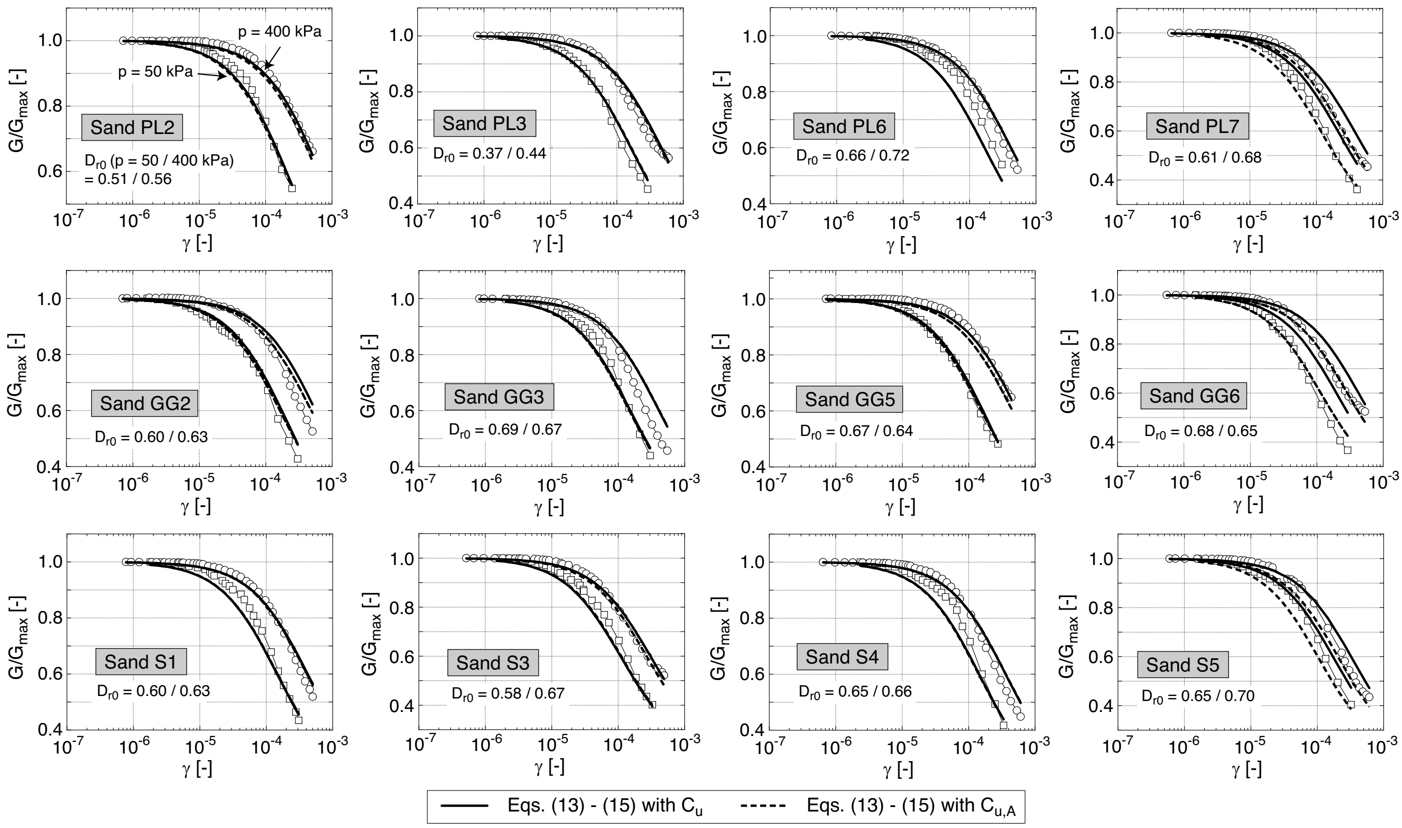

Fig. 12: *Shear modulus degradation curves $G(\gamma)/G_{\max}$ for stepwise-linear (first row), gap-graded (second row) and smoothly shaped (third row) grain size distribution curves. The experimental data is compared to the $G(\gamma)/G_{\max}$ curves predicted by Eqs. (13) to (15). The correlations have been applied either with C_u (solid curves) or $C_{u,A}$ (dashed curves). (Figure 4 from [12] supplemented by the dashed curves)*

from tests on linear gradations are applied with an average inclination $C_{u,A}$ of the grain size distribution curve instead of C_u.

5 Poisson's ratio

Poisson's ratio ν can be calculated from

$$\nu = \frac{\alpha}{4(1-\alpha)} + \sqrt{\left(\frac{\alpha}{4(1-\alpha)}\right)^2 - \frac{\alpha-2}{2(1-\alpha)}} \qquad (16)$$

with $\alpha = M_{\max}/G_{\max}$. The experimental ν data at pressures p = 100 and 400 kPa is presented in Figure 13. It confirms the slight decrease of ν with increasing confining pressure reported in [10]. Furthermore, for most tested materials a moderate increase of Poisson's ratio with increasing void ratio was measured. In Figure 13, the prediction of Eq. (16) with $G_{\max}$ from Eqs. (9) to (12) and $M_{\max}$ from Eqs. (1) to (4) has been added as solid or dashed curves, respectively. The solid curves in Figure 13 have been obtained with C_u as input for the correlations while the dashed curves have been generated using $C_{u,A}$. The prediction for both, C_u and $C_{u,A}$, reflects the measured increase of ν with decreasing pressure and increasing void ratio. For most tested sands, the predicted Poisson's ratios are close to the measured data if C_u is used in the correlations. However, for some of the sands, in particular PL7, GG6 and S3, the ν prediction is significantly improved if the correlations are applied with the average inclination $C_{u,A}$.

6 Conclusions

Approx. 120 resonant column (RC) tests with additional P-wave measurements have been performed on 19 clean quartz sands with piecewise linear, gap-graded or smoothly shaped grain size distribution curves. For each material the P-wave velocity was measured at different densities and pressures. Similar as in an earlier test series on linear grain size distribution curves [10], a significant decrease of the constrained elastic modulus $M_{\max}$ with increasing uniformity coefficient C_u of the grain size distribution curve was also observed for the more complex gradations tested in the present study.

The applicability of the empirical equations (1) to (4) for $M_{\max}$ was inspected for the more complex grain size distribution curves. These correlations proposed by the authors in [10] are based on data for linear grain size distribution curves and consider the decrease of $M_{\max}$ with C_u for constant values of pressure and void ratio. Based on the present test data it could be demonstrated that the new correlations work well also for more complex grain size distribution curves. The prediction can be somewhat improved if the new correlations are applied with an average inclination $C_{u,A}$ of the grain size distribution curve (see the scheme in Figure 9) instead of C_u, in particular in the case of materials that are primarily composed of two components with significantly different grain size. For most practical cases, however, it may suffice to use the conventional C_u as input for the correlations.

A reanalysis of the data of small-strain shear modulus

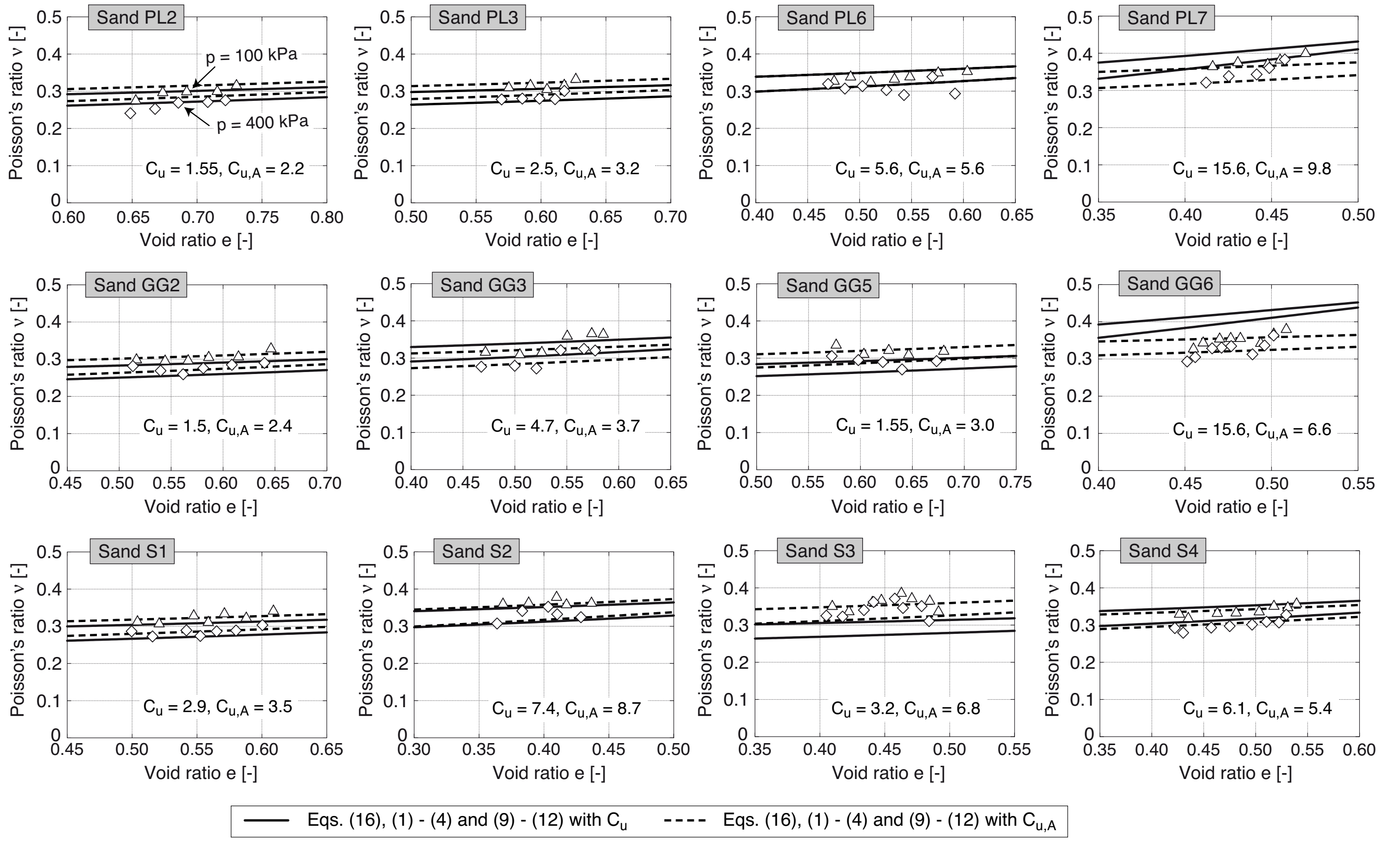

Fig. 13: *Poisson's ratio ν at pressures p = 100 and 400 kPa for stepwise-linear (first row), gap-graded (second row) and smoothly shaped (third row) grain size distribution curves. The experimental data is compared to the Poisson's ratio predicted by Eq. (16) with $G_{\max}$ from Eqs. (9) to (12) and $M_{\max}$ from Eqs. (1) to (4). The correlations have been applied either with C_u (solid curves) or $C_{u,A}$ (dashed curves).*

$G_{\max}$ and modulus degradation ratio $G(\gamma)/G_{\max}$ for the piecewise linear, gap-graded and smoothly shaped grain size distribution curves provided in [12] revealed that the $G_{\max}$ and $G(\gamma)/G_{\max}$ predictions for some of these sands can also be improved if the respective correlations derived from tests on linear gradations [9, 11] are applied with an average inclination $C_{u,A}$ instead of C_u. The same applies to Poisson's ratio ν which has been analyzed based on the measured $M_{\max}$ and $G_{\max}$ data.

Finally, it should be stressed that the extended empirical equations for $M_{\max}$, $G_{\max}$ and $G(\gamma)/G_{\max}$ are confirmed for clean sands with C_u-values less than 16 only. Therefore, until additional experimental data are available, they should be only applied within this range.

Acknowledgements

The presented study has been performed within the framework of the project "Influence of the grain size distribution curve on the dynamic properties of non-cohesive soils" funded by the German Research Council (DFG, project No. TR 218/17-1). The authors are grateful to DFG for the financial support.

References

[1] S.S. Afifi and Jr. Richart, F.E. Stress-history effects on shear modulus of soils. *Soils and Foundations*, 13(1):77–95, 1973.

[2] S.S. Afifi and R.D. Woods. Long-term pressure effects on shear modulus of soils. *Journal of the Soil Mechanics and Foundations Division, ASCE*, 97(SM10):1445–1460, 1971.

[3] C.D.P. Baxter. *An experimental study on the aging of sands.* PhD thesis, Faculty of the Virginia Polytechnic Institute and State University, July 1999.

[4] G.M. Brignoli, M. Gotti, and K.H. II. Stokoe. Measurement of shear waves in laboratory specimens by means of piezoelectric transducers. *Geotechnical Testing Journal, ASTM*, 19(4):384–397, 1996.

[5] B.O. Hardin and W.L. Black. Sand stiffness under various triaxial stresses. *Journal of the Soil Mechanics and Foundations Division, ASCE*, 92(SM2):27–42, 1966.

[6] B.O. Hardin and V.P. Drnevich. Shear modulus and damping in soils: design equations and curves. *Journal of the Soil Mechanics and Foundations Division, ASCE*, 98(SM7):667–692, 1972.

[7] B.O. Hardin and F.E. Richart Jr. Elastic wave velocities in granular soils. *Journal of the Soil Mechanics and Foundations Division, ASCE*, 89(SM1):33–65, 1963.

[8] T. Iwasaki and F. Tatsuoka. Effects of grain size and grading on dynamic shear moduli of sands. *Soils and Foundations*, 17(3):19–35, 1977.

[9] T. Wichtmann and T. Triantafyllidis. On the influence of the grain size distribution curve of quartz sand on the small strain shear modulus $G_{\max}$. *Journal of Geotechnical and Geoenvironmental Engineering, ASCE*, 135(10):1404–1418, 2009.

[10] T. Wichtmann and T. Triantafyllidis. On the influence of the grain size distribution curve on P-wave velocity, constrained elastic modulus $M_{\max}$ and Poisson's ratio of quartz sands. *Soil Dynamics and Earthquake Engineering*, 30(8):757–766, 2010.

[11] T. Wichtmann and T. Triantafyllidis. Effect of uniformity coefficient on $G/G_{\max}$ and damping ratio of uniform to well graded quartz sands. *Journal of Geotechnical and Geoenvironmental Engineering, ASCE*, 139(1):59–72, 2013.

[12] T. Wichtmann and T. Triantafyllidis. Stiffness and damping of clean quartz sand with various grain size distribution curves. *Journal of Geotechnical and Geoenvironmental Engineering*, 140(3), 2014.

[13] T. Wichtmann and Th. Triantafyllidis. Influence of a cyclic and dynamic loading history on dynamic properties of dry sand, part II: cyclic axial preloading. *Soil Dynamics and Earthquake Engineering*, 24(11):789–803, 2004.

[14] P. Yu and F.E. Richart Jr. Stress ratio effects on shear modulus of dry sands. *Journal of Geotechnical Engineering, ASCE*, 110(3):331–345, 1984.